Stopping power of fluorides and semiconductor organic films for low-velocity protons

L. N. Serkovic Loli,* E. A. Sánchez, O. Grizzi, and N. R. Arista
Centro Atómico Bariloche—CNEA, Instituto Balseiro–UNCuyo, CONICET 8400 S. C. de Bariloche, Río Negro, Argentina
(Received 16 November 2009; published 16 February 2010)

A combined experimental and theoretical study of the energy loss of protons in fluorides and organic films is presented. The measurements were performed in fresh AlF_3, LiF, and N,N'-bis(1-ethylpropyl)-perylene-3,4,9,10-tetracarboxdiimide (EP-PTCDI) evaporated *in situ* on self-supported C or Ag foils, covering the very low energy range from 25 keV down to 0.7 keV. The transmission method is used in combination with time-of-flight (TOF) spectrometry. In the case of fluorides with large band gap energies (AlF_3 and LiF), the experimental stopping power increases almost linearly with the mean projectile velocity showing a velocity threshold at about 0.1 a.u. These features are well reproduced by a model based on quantum scattering theory that takes into account the velocity distribution and the excitation of the active $2p$ electrons in the F^- anions, and the properties of the electronic bands of the insulators. In the case of the semiconductor organic film with a lower gap, the experimental stopping power increases linearly with the mean projectile velocity without presenting a clear threshold. This trend is also reproduced by the proposed model.

DOI: 10.1103/PhysRevA.81.022902 PACS number(s): 34.50.Bw, 78.20.Bh

I. INTRODUCTION

The stopping of ions propagating through matter has been a subject of investigation over the last century [1,2]. The interest on the stopping power is based on many applications in materials science, radiation physics, and medical physics [3]. More recently, with the development of fast electronics, which require semiconductor devices produced by shallow ion implantation, its knowledge at low ion velocities and for different materials has become critical.

It has been very well established from the experimental and theoretical point of views that for low projectile velocities (<1 a.u.), the main stopping mechanism in metals is due to the excitation of valence electrons. Modeling these electrons as a free electron gas, the calculated stopping power shows a well-known proportional dependence with ion velocity, observed also in experiments. For the case of noble metals (Au, Ag, and Cu) [4], where the density of states is formed by an intense and narrow band of d electrons located below the Fermi energy, and a weaker and broader band of s and p electron states filled up to the Fermi energy, the stopping power can be separated into two contributions: one corresponding to the free s and p electrons whose dependence on projectile velocity looks like jellium-type metals, and the other one corresponding to loosely bound d electrons that increases linearly but would start from a finite velocity threshold [5,6].

For the case of insulators, a linear behavior with a more discernible velocity threshold was observed experimentally in grazing scattering of protons from flat LiF surfaces [7] and in backscattering of protons from LiF films evaporated on Au substrates [8]. More recently, an unambiguous velocity threshold at about 0.1 a.u. was measured for protons transmitted through AlF_3 thin films evaporated on self-supported C foils [9] and for proton, deuteron, and helium ions backscattered from LiF and KCl thin films [10].

From the theoretical point of view, there are few models that have been proposed to describe such behavior. Boudjema *et al.* [11] presented a density functional theory (DFT) model following the binary collision approximation for the energy loss of light particles scattered by solid surfaces at low energy that includes the presence of the energy gap. This model shows a deviation from the velocity proportionality of the stopping power of Si and Ge for velocities below 0.3 a.u. Pruneda *et al.* [12] presented another model, also based on DFT calculations, that describes a velocity threshold of 0.2 a.u. for LiF which is still higher than the one observed experimentally ($\sim$0.1 a.u.), and a stopping power value which is half of the experimental one. In a previous work [9], we presented another model based on quantum scattering theory that takes into account the velocity distribution and the excitation of the active $2p$ electrons in the F^- anions, and the properties of the electronic bands of the insulators. This model described the general trends and the measured velocity threshold of 0.1 a.u. of the proton stopping power on AlF_3.

In this work, we present new experimental data for the stopping power of very low velocity protons that traverse large band-gap inorganic insulating (LiF, AlF_3) and low band-gap organic semiconducting (N,N'-bis(1-ethylpropyl)-perylene-3,4,9,10-tetracarboxdiimide: EP-PTCDI – $C_{34}H_{30}N_4O_2$) thin films evaporated on self-supported C and Ag films. The behavior of the experimental stopping powers as a function of proton velocity is discussed and compared with the predictions of our theoretical model [9] based on calculations of the momentum transfer cross sections for the electron-ion collisions using quantum scattering methods, which incorporates the energy gap of the insulators and the organic semiconductor materials, and the velocity distributions of their corresponding active electrons. We also compared the experimental stopping powers with a model for compounds that includes Bragg additivity's rule [13] and the core and bond approach [14].

II. EXPERIMENTAL AND THEORETICAL METHODS

A. Experiment

The measurements of the energy loss were performed by combining the transmission method with time-of-flight (TOF)

*serkovic@cab.cnea.gov.ar

analysis through very thin layers of LiF, AlF_3, or EP-PTCDI evaporated on self-supported carbon or silver foils under ultra-high-vacuum (UHV) conditions.

In the transmission method, we measure the particles that traverse a thin foil at a scattering angle of 0°. Within this experimental condition, the multiple scattering processes do not contribute to the measured spectra because strong interactions with the target nucleus will cause the particles to be emitted at larger angles, out of the detector acceptance. If we start with a very well collimated beam incoming at normal incidence with respect to the foil surface, the path length of the particle within the solid will be the thickness of the foil. So, the determination of the stopping power is simply the energy loss divided by the foil thickness. This method is much more straightforward than the one used in backscattering conditions [8,10] because it is not necessary to simulate the energy spectra obtained from multiple scattering collisions through unknown trajectories.

The TOF technique allows measurements of stopping powers with fluences as low as 10^{10} ions/cm^2 per spectrum, thus producing only undetectable damage on the evaporated films. This was corroborated by the concordant results obtained on the same target at the beginning and at the end of the extended measurement series. The detail of the experimental method can be found in Ref. [9].

The C foils of nominally 4 μ g/cm^2 thickness were bought from ACF Metals [15]. Its thickness was measured with a calibrated Autoprobe CP Atomic Force Microscope (AFM) from Park Scientific Instruments and by normalizing the energy loss results taken at 9 keV with the stopping power values obtained with the SRIM 2006 code [16]. The result was a thickness of 280 Å. Two Ag foils of different thicknesses were made by the technique of evaporation on a plastic backing, which is subsequently dissolved [17]. Thicknesses of 225 and 170 Å were measured by comparing the energy loss results for each foil with previous stopping power data obtained by Valdés *et al.* [4].

Fluorides and EP-PTCDI depositions were performed *in situ* from a Knudsen cell charged with LiF, AlF_3, or EP-PTCDI on the C or Ag foils. The cell was carefully degassed and shuttered to avoid sample contamination. Pressures in the 10^{-9} Torr range were kept throughout the evaporation and the measurements. The deposition speed and the evaporated mass were monitored by a quartz crystal balance of a known aperture (3 mm) placed on the sample holder. The quality of the AlF_3 film was checked with the AFM giving a uniform film with an rms roughness (root-mean-square deviation of the height histogram) of 7 Å for a 1-μm^2 area. To measure the thickness, the evaporation was performed on a flat substrate (rms $<$ 3 Å) with a mask placed in front of it. The step height of the interface between the AlF_3 film and the substrate was then measured with the AFM giving an average value of the AlF_3 film thickness of 230 $\pm$ 50 Å. The error in the thickness determination was obtained from the statistical distribution of the height values measured in the interface. This allowed us to measure the density of the evaporated film (2.7 g/cm^3), which is similar to that of the bulk material (3.1 g/cm^3). The quality and thickness of the LiF film were also checked with the AFM, giving a uniform film with an rms roughness of 7 Å for a 1-μm^2 area, with a thickness of 275 $\pm$ 40 Å, and a film density of 1.9 g/cm^3, somewhat lower than its bulk density (2.6 g/cm^3). Finally, for the EP-PTCDI organic film, the AFM images showed that the molecules grow forming islands of different sizes that do not coalesce completely, therefore, leaving some very small parts of the substrate uncovered [18]. The quality of the films was checked with the AFM giving an rms roughness of 56 Å. The mean thickness for both evaporations over the C and Ag foils was measured with the crystal quartz balance giving a value of 210 Å and a film density of 1.5 g/cm^3. The film density was also checked using the atomic mass of the molecule per volume of the unit cell obtained in a previous work [18,19] with a scanning tunneling microscope.

B. Theory of stopping power for compounds

Bragg and Kleeman studied the energy loss of alpha particles in hydrocarbon gases to find out the stopping dependence on the atomic weight of the target [20]. From this work, in 1905 they proposed the Bragg additivity's rule [8] that states that the stopping of a compound may be estimated by the linear combination of the stopping cross sections of its individual elements:

$$S_{\mathrm{Bragg}} = \sum_n c_n S_n, \tag{1}$$

where c_n and S_n are the number of atoms per molecule and the stopping cross section of the element n, respectively. The stopping cross section, S, is related to the stopping power, $-dE/dx$, by the equation $S = -(1/N)dE/dx$, where N is the atomic density of the target material.

Bragg additivity's rule is limited because the electronic energy loss in any material depends on the detailed orbital and excitation structure of the matter. Therefore, any difference between elemental materials and the same atoms in compounds will cause Bragg additivity's rule to become inaccurate. Also, the chemical bonding in the compounds may also alter the charge state of the ion, changing the strength of its interaction with the target medium. For projectile energies above the stopping power maximum, the Bragg rule works well; however, for lower energies, important deviations have been found. This is due to the fact that at lower energies, the stopping power is dominated by the valence electrons that are more sensitive to the chemical environment of the compound.

To mend these uncertainties, we use the core and bond (CAB) approach [20] that proposes to treat the problem by reducing each target atom into two parts: the core electrons which are unperturbed by the bonds in the compound and the bonding electrons. The unperturbed part follows Bragg's rule, and the electronic bonding part includes the chemical bonds of the compound for the stopping correction. The CAB approach has reproduced very well the stopping values for organic compounds such as ethylene and polystyrene [21], so we expect that it will also reproduce our results on EP-PTCDI. For this case, we have to add the chemical bonds between the different elements in the molecule which are 26 of C–C, 10 of C=C, 30 of C–H, 6 of C–N, and 4 of C=O.

In order to compute this model, we use Ziegler's SRIM 2006 code [22] that includes the CAB approach and follows Bragg additivity's rule by specifying the stoichiometry and the bonds within the compound. A limitation of the SRIM code

is that it only takes into account the bonds of light elements, especially for hydrocarbons, and it does not include any Li or Al bond; so for the fluorides, it will only calculate the stopping power following Bragg additivity's rule and will not include the CAB correction. Within this approximation, the energy gap for large band gap materials is not taken into account, so the threshold observed at very low projectile velocities is not reproduced. Therefore, different models have to be developed to account for this observation.

C. Generalized model for low-velocity projectiles

Due to the zero exit angle of our experimental geometry, only electronic excitations will be taken into account in the theoretical analysis of the energy loss; strong interactions with the target nucleus will cause the particles to be emitted at larger angles, out of the detector acceptance. The electronic excitations are caused by the ion that passes through the material, disturbing the valence electrons.

The theoretical method has already been described in a recent work [9], where we have calculated the stopping power just considering the $2p$ F^- velocity distribution for the case of the fluorides. In this work, we have extended the calculations for different mean velocity values corresponding to the $2s$ and $2p$ F^- velocity distribution in the case of fluorides, as well as for carbon and EP-PTCDI films. The model considers that the interaction of a moving ion with target electrons produces stopping forces which, for velocities $v < v_0$ (with $v_0 =$ Bohr velocity), may be expressed as

$$-\frac{dE}{dx} = Qv, \tag{2}$$

where Q is the value of the stopping coefficient. The energy loss expression of Eq. (2) contains a velocity-dependent stopping coefficient given by

$$Q = \frac{4\pi}{3} n \int_0^\infty v_e^4 \sigma_{tr}^*(v, v_e, U) \left[\frac{-dF(v_e)}{dv_e}\right] dv_e, \tag{3}$$

where $F(v_e)$ is the electron velocity distribution. In this model, the transport cross section has been modified in order to take into account a possible energy threshold U in the electronic excitations. For this purpose, we defined a *restricted* transport cross section σ_{tr}^* by

$$\begin{aligned}\sigma_{tr}^* &= \sigma_{tr}^*(v, v_r, U) \\ &= 2\pi \int_{\theta_{\min}(v,v_r,U)}^{\pi} |f(\theta)|^2 (1 - \cos\theta) \sin\theta d\theta,\end{aligned} \tag{4}$$

where we have introduced a minimum scattering angle $\theta_{\min}$, and $f(\theta)$ is the scattering amplitude given by

$$f(\theta) = \frac{\hbar}{m v_r} \sum_l (2l+1) e^{i\delta_l} \sin(\delta_l) P_l(\cos\theta). \tag{5}$$

Here v_r and θ are the relative ion-electron velocity and the scattering angle in the center-of-mass (c.m.) system and δ_l is the phase shift corresponding to the scattering of waves with angular momentum l.

In the case of materials with a finite energy gap U, we have to take into account only those processes that provide energy transfers $\Delta E \geqslant U$. The relation between $\theta_{\min}$ and U may be obtained by considering that a scattering angle θ is associated with an energy transfer ΔE in the laboratory system given by

$$\Delta E(\theta) = m v v_r (1 - \cos\theta). \tag{6}$$

Therefore, the minimum scattering angle $\theta_{\min}$, corresponding to energy transfers larger than U, is determined by the condition $\Delta E(\theta_{\min}) = U$, which yields $\cos\theta_{\min} = 1 - U/mvv_r$. The energy gaps for LiF, AlF_3, and EP-PTCDI are 14, 10.8 [9], and ~2 eV [18], respectively.

For the case of ionic compounds like AlF_3 and LiF, the valence band is formed by the $2s$ and $2p$ orbitals of the F^- anion. Taking into account the atomic-like character of these orbitals, the electron velocity distribution $F(v_e)$ has been calculated using the method described by Ponce in Ref. [23] and using Clementi and Roetti's values from Ref. [24]. For the case of the EP-PTCDI organic molecule, we took into account the H $1s$, C $2s$ and $2p$, N $2p$, and O $2p$ electrons to determine the electron density ($n = 0.047$ a.u.) and the electron velocity distribution.

For the phase shifts δ_l, we have used two different approaches. One that considers the stopping medium as an homogeneous electron gas and calculates the values of δ_l for each ion atomic number Z_1 using the DFT [25]. Following this approximation, we used the tabulated results for the phase shifts obtained by Puska and Nieminen [25] using the r_s values of the different materials (1.446, 1.5, and 1.7 a.u. for AlF_3, LiF, and EP-PTCDI, respectively). The second method to calculate the phase shifts consists of performing a numerical integration of the radial Schrödinger's equation within a nonlinear approach (NLA) described in Ref. [26], using different mean electron velocities representatives of the electron velocity distributions. The velocities used for AlF_3 and LiF were from 1.1 a.u. [the maximum in the velocity distribution $F(v_e)$], up to 1.9 a.u. (the mean velocity of the F^- electrons). For the EP-PTCDI molecule, the velocities were between 1.2 a.u. [the mean velocity of $F(v_e)$] and 1.6 a.u. [the quadratic mean velocity of $F(v_e)$].

III. RESULTS AND DISCUSSION

A. Fluoride films

The TOF spectra were measured for the direct beam, for the beam transmitted through the C self-supporting foils, and through the C foil with a layer of evaporated fluorides (LiF or AlF_3). The projectile energies ranged from 0.7 to 28 keV. The TOF spectra were converted to energy distributions to allow the determination of their energy positions in order to evaluate the energy loss values. A set of spectra taken for 2.9-keV protons on LiF are shown in Fig. 1. Those obtained for AlF_3 can be seen in Fig. 1 of Ref. [9]. The energy spectra were fitted by simple Gaussian curves which accurately reproduced the peak energies, allowing a precise determination of the energy losses.

The measured energy losses as a function of the incoming energy for LiF are presented in Fig. 2 (energy loss results for AlF_3 are presented in Fig. 2 of Ref. [9]). The data were obtained in the following way: First, the energy loss on the substrate foil as a function of the primary incoming proton energy E_0 was obtained, and the data were fitted with a polynomial curve; and second, the total energy loss (substrate foil + evaporated film)

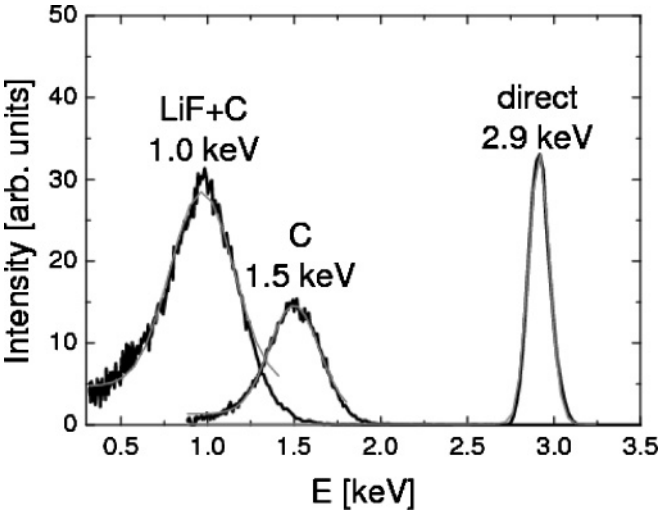

FIG. 1. Energy spectra for 2.9-keV protons passing through a carbon foil and through the carbon foil + evaporated LiF film. The energy spectrum for the corresponding direct beam is also shown.

was measured as a function of E_0, and the difference between these data and the polynomial fit provided the energy loss in the evaporated film. Each data set is then plotted versus the corresponding incoming proton energy in each layer (E_0 for the substrate foil and for the substrate + evaporated foil, and E_1 for the evaporated film alone).

The dependencies of the stopping power for LiF and for AlF_3 as a function of the mean projectile velocity are shown in Fig. 3. The experimental method used in this work allowed us to extend the measurements of the stopping power on fluorides down to ∼0.1 a.u., showing a clear threshold around this velocity, and a linear dependence for higher velocities.

A comparison of the experimental data of AlF_3 and LiF with our calculations using both phase shift methods is presented in Fig. 3 together with the semiempirical values from the SRIM

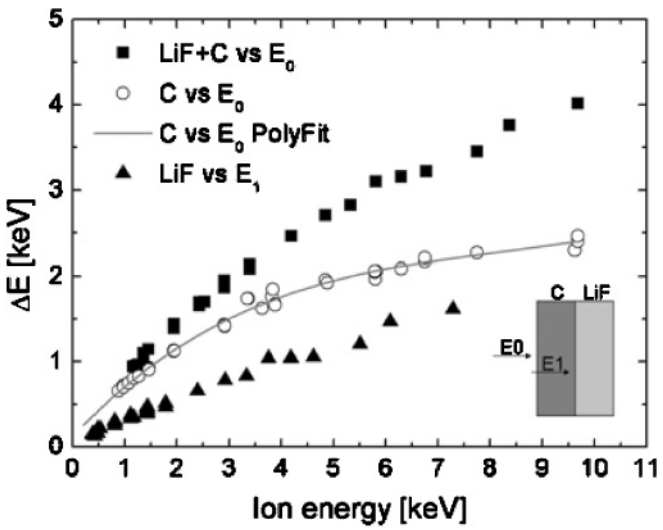

FIG. 2. Energy loss measured in C and C + LiF thin foils. The line corresponds to a polynomial fit of the energy loss in C. The energy loss for LiF has been obtained by subtracting the C polynomial fit from the C + LiF values.

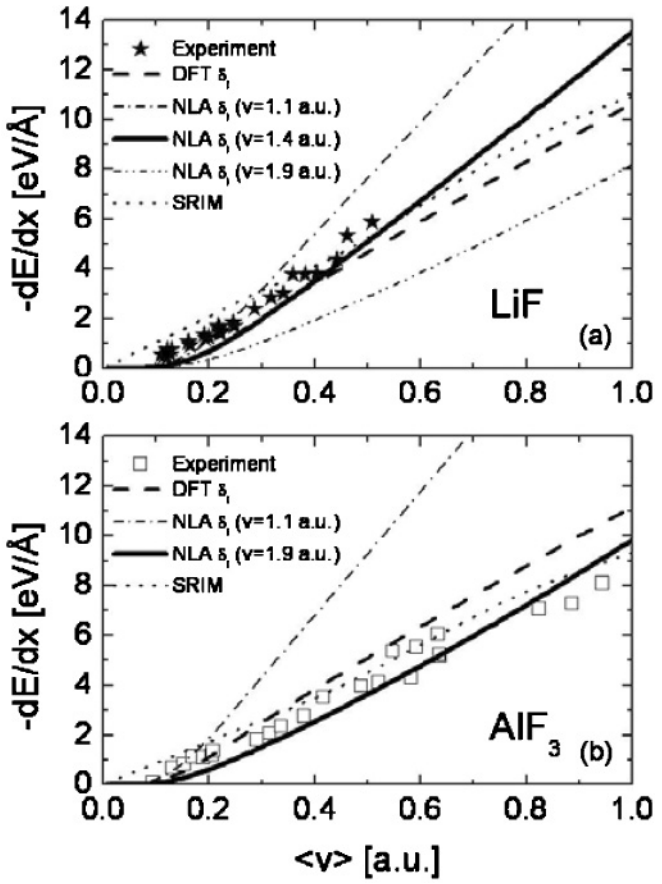

FIG. 3. Stopping power values for (a) LiF and (b) AlF_3 measured as a function of the mean projectile velocity. The lines show the calculations of the stopping power using the phase shifts taken from the DFT model and from the NLA using the mean velocities indicated in each panel. The stopping power values obtained for compounds with the SRIM code are also shown.

code using the Bragg additivity's rule. The velocities used for the calculation of the atomic phase shifts ranged from 1.1 to 1.9 a.u., which correspond to the maximum of the velocity distribution $F(v_e)$ and the mean velocity of the $2s$ and $2p$ F^- electrons, respectively. The best agreements between the calculated and the experimental values for LiF and AlF_3 were obtained for 1.4 and 1.9 a.u., respectively.

The comparison between the experimental and theoretical results shows a close agreement for the absolute values and the general behavior of the stopping power versus projectile velocity. Another important result is that the values of the velocity thresholds can be well reproduced by the present model. As expected, the SRIM results for fluorides with large energy band gaps do not account for the velocity threshold, but for higher velocities (above ∼0.3 a.u.), it does reproduce fairly well the stopping values for both fluorides.

In Fig. 4, we present the stopping cross sections per atom for LiF and AlF_3 obtained from the experimental stopping power values using atomic densities of 1.22 and 0.89×10^{23} atoms/cm^3, respectively. We have also included in Fig. 4 the stopping cross sections per atom obtained from Refs. [8] and [10] for the LiF case. For all these fluorides, the results are very similar, in agreement with the assumption that for

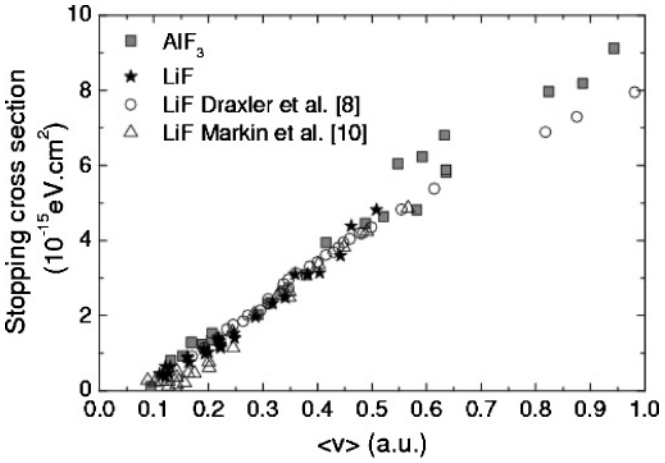

FIG. 4. Stopping cross sections per atom as a function of the mean projectile velocity are shown for LiF and AlF_3 samples, together with LiF results from Refs. [8] and [10].

ionic insulators the behavior of the stopping at low energies is dominated by the $2s$ and $2p$ electrons [27] provided by the F^- anions.

B. EP-PTCDI organic film

In the case of the organic compound, the TOF spectra were also measured for the direct beam, for the beam transmitted through the substrate self-supporting foils (C or Ag), and through the substrate foil with a layer of evaporated EP-PTCDI. The projectile energies ranged from 1 to 13 keV. The corresponding energy spectra obtained for 5.8-keV protons are shown in Fig. 5. The ones obtained for the direct beam, and the beam passing through the C foil look similar to those shown previously for the fluorides, but the energy spectrum obtained for the EP-PTCDI + C film presents two peaks: one centered at the energy corresponding to the C foil previous to the EP-PTCDI deposition, and the second one, much broader and centered at lower energies. The

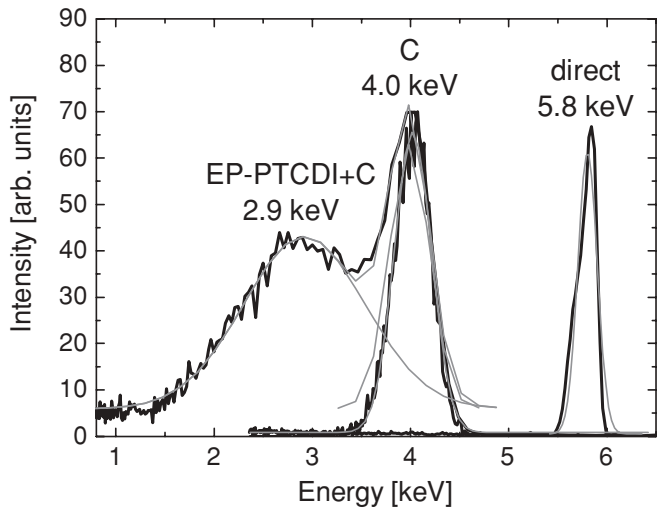

FIG. 5. Energy spectra for 5.8-keV protons passing through a carbon foil and through the carbon foil + EP-PTCDI film. The energy spectrum for the corresponding direct beam is also shown.

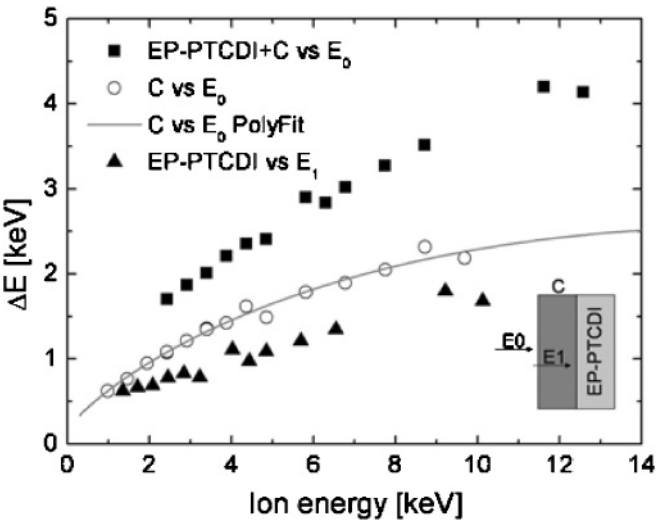

FIG. 6. Energy loss measured in C foil and C + EP-PTCDI thin film. The line corresponds to the polynomial fit of the energy loss in C. The energy loss for EP-PTCDI has been obtained by subtracting the C polynomial fit from the C + EP-PTCDI values.

first one corresponds to protons transmitted through part of the sample that was not covered by the molecules, and the second one to the rougher EP-PTCDI film, in agreement with the topographic measurements performed by the AFM [18]. The superposition of the peaks for lower proton energies did not allow the determination of the energy loss for incident proton energies (E_0) lower than 1 keV, precluding the observation of an eventual threshold effect. The attempts to grow smoother EP-PTCDI films on different substrates like Ag foils and to vary the evaporation conditions were not successful.

The summary of the measured energy loss as a function of the incoming energy for EP-PTCDI on carbon is presented in Fig. 6. This data were obtained in the same way as for the LiF results.

Figure 7(a) shows the results of the experimental stopping power of C and of EP-PTCDI evaporated on C and Ag self-supporting thin foils versus the mean projectile velocity. The experimental results are also compared with the SRIM results obtained following the Bragg model and the CAB approximation. Both calculations performed by the SRIM code describe quite well the results for EP-PTCDI, giving just a small difference between the Bragg model and the CAB approach at $\langle v \rangle = 0.6$ a.u. of about 1.5%, and an underestimation of the stopping power value of about 10%. For the case of C, the SRIM code also reproduces fairly well the experimental results overestimating the stopping power values just about 7%.

We also tested the results of our model with the semiconductor organic film that presents an energy band gap lower than the fluoride case. In Fig. 7(b), we show the calculations of the stopping power versus the mean projectile velocity performed using the two different approaches for the phase shift evaluation. For the phase shifts calculated by the integration of the radial Schrödinger's equation, we show the results obtained for 1.2 and 1.6 a.u. velocities which correspond to the mean velocity of $F(v_e)$ and the quadratic mean velocity of $F(v_e)$, respectively. The last one gives the

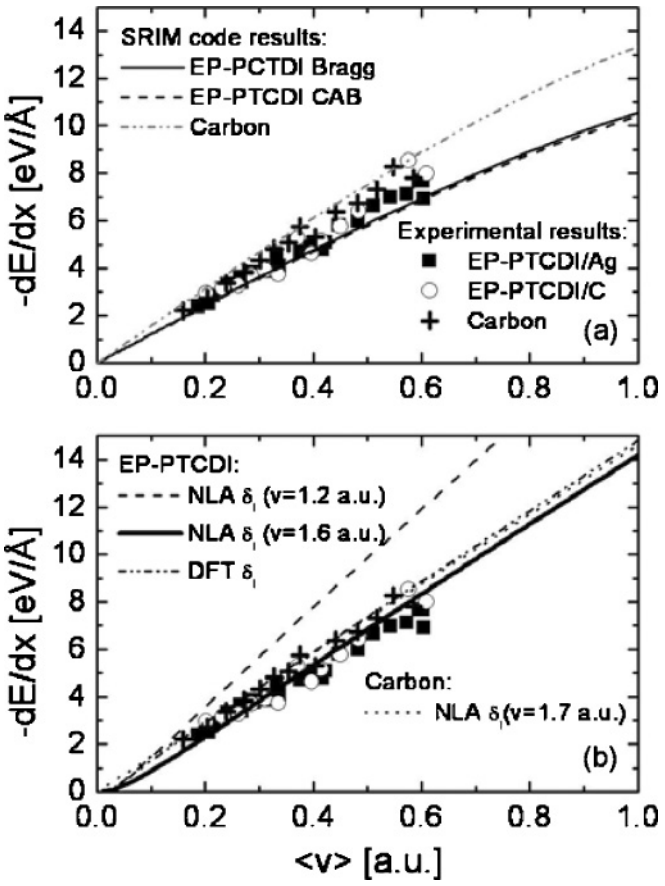

FIG. 7. Stopping power values for EP-PTCDI on Ag and C foils measured as a function of its mean projectile velocity compared with (a) the stopping power model for compounds (SRIM results) and (b) our model for different phase shifts. Experimental and theoretical results for C are also shown.

best agreement (less than 6% difference), predicting a velocity threshold of about 0.02 a.u. that could not be achieved with the experimental results because of the particular characteristics of the EP-PTCDI films (very large roughness with grains that do not completely coalesce) as explained in the Experimental section. The calculation performed with the DFT phase shifts gave similar but slightly higher results.

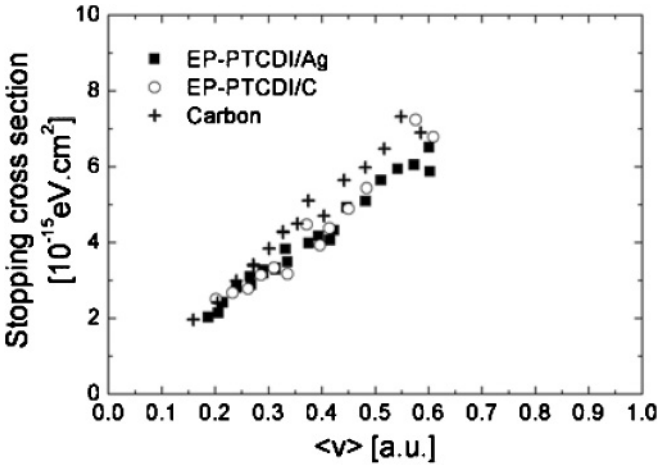

FIG. 8. Stopping cross sections per atom as a function of the mean projectile velocity for EP-PTCDI and C.

The calculation for the stopping power of carbon was also performed, using $r_s = 1.66$ a.u. and a velocity of 1.7 a.u. to calculate the atomic phase shifts in the NLA approximation. These results are compared with those obtained experimentally giving a very good agreement, better than with the SRIM code results.

For completeness, in Fig. 8, we also present the stopping cross sections per atom for EP-PTCDI and C calculated using atomic densities of 1.18 and 1.13×10^{23} atoms/cm^3, respectively. Both stopping cross sections are similar, probably due to the high contribution of carbon atoms to the stopping power in the EP-PTCDI molecule.

IV. CONCLUSIONS

These stopping power measurements for low-velocity protons traversing LiF and AlF_3 thin films show a well-defined threshold at 0.1 a.u. and, from this value, an almost linear increase with the mean projectile velocity. For the EP-PTCDI organic molecules, the measurements follow a similar behavior, but we could not observe the predicted smaller velocity threshold (0.026 a.u.) because of the limitation of the minimum velocity achieved due to the particular morphology of the films.

The experimental results were compared with the results obtained with the SRIM code using Bragg additivity's rule and the core and bond approach to account for the compounds. The general behavior was reproduced for proton mean velocities higher than ~0.3 a.u. for the fluorides and ~0.2 a.u. for the organic molecules. No thresholds were obtained with this model.

To account for the velocity thresholds observed in materials with an energy gap in the local electronic density of states, we have developed a free parameter model that considers the excited valence electrons as free but with a restriction in the transport cross section that includes the minimum energy transfer due to the presence of the gap. This model has been previously used to reproduce the measured stopping power on AlF_3, and here we have extended its application to describe the experimental results of AlF_3, LiF, EP-PTCDI, and C. This model reproduces fairly well the general trends and the stopping power values in all the studied materials that include large band-gap insulators, low band-gap semiconductors, as well as carbon. The velocity threshold measured for the fluorides was also well reproduced by the model.

ACKNOWLEDGMENTS

The authors acknowledges many stimulating discussions with Drs. G. H. Lantschner and J. C. Eckardt, and partial financial support from ANPCyT (PICT 2006 03–715 and PICT 903/07), CONICET (PIP N° 112–200801-00958), and Universidad Nacional de Cuyo (06-C317 and 06-C323).

[1] J. Lindhard, K. Dan. Vidensk. Selsk. Mat.-Fys. Medd. **28**, 1 (1954).
[2] T. L. Ferrell and R. H. Ritchie, Phys. Rev. B **16**, 115 (1977).
[3] H. Paul, O. Geithner, and O. Jäkel, Nucl. Instrum. Methods B **256**, 561 (2007).
[4] J. E. Valdés, J. C. Eckardt, G. H. Lantschner, and N. R. Arista, Phys. Rev. A **49**, 1083 (1994).
[5] E. A. Figueroa, E. D. Cantero, J. C. Eckardt, G. H. Lantschner, J. E. Valdés, and N. R. Arista, Phys. Rev. A **75**, 010901(R) (2007).
[6] E. D. Cantero, G. H. Lantschner, J. C. Eckardt, and N. R. Arista, Phys. Rev. A **80**, 032904 (2009).
[7] C. Auth, A. Mertens, H. Winter, and A. Borisov, Phys. Rev. Lett. **81**, 4831 (1998).
[8] M. Draxler, S. P. Chenakin, S. N. Markin, and P. Bauer, Phys. Rev. Lett. **95**, 113201 (2005).
[9] L. N. Serkovic, E. A. Sánchez, O. Grizzi, J. C. Eckardt, G. H. Lantschner, and N. R. Arista, Phys. Rev. A **76**, 040901(R) (2007).
[10] S. N. Markin, D. Primetzhofer, and P. Bauer, Phys. Rev. Lett. **103**, 113201 (2009).
[11] M. Boudjema, N. D'bichi, Y. Boudouma, A. C. Chami, B. Arezki, K. Khalal, C. Benazeth, and P. Benoit-Cattin, Nucl. Instrum. Methods B **164-165**, 588 (2000).
[12] J. M. Pruneda, D. Sánchez-Portal, A. Arnau, J. I. Juaristi, and E. Artacho, Phys. Rev. Lett. **99**, 235501 (2007).
[13] W. H. Bragg and R. Kleeman, Philos. Mag. **10**, 318 (1905).
[14] G. Both, R. Krotz, K. Lohmer, and W. Neuwirth, Phys. Rev. A **28**, 3212 (1983).
[15] ACF Metals—Arizona Carbon Foil Co. Inc., 2239 East Kiendale Road, Tucson, Arizona 85719, USA.
[16] J. F. Ziegler, M. D. Ziegler, and J. P. Biersack, Computer code SRIM 2006.02 (2006); http:/www.srim.org.
[17] A. Valenzuela and J. C. Eckardt, Rev. Sci. Instrum. **42**, 127 (1971).
[18] L. N. Serkovic Loli, H. Hamoudi, J. E. Gayone, M. L. Martiarena, E. A. Sánchez, O. Grizzi, L. Pasquali, S. Nannarone, B. Doyle, C. Dablemont, Céline, and V. A. Esaulov, J. Phys. Chem. C **113**, 17866 (2009).
[19] L. N. Serkovic Loli, E. A. Sánchez, J. E. Gayone, O. Grizzi, and V. A. Esaulov, Phys. Chem. Chem. Phys. **11**, 3849 (2009).
[20] W. H. Bragg and R. Kleeman, Philos. Mag. **8**, 726 (1904).
[21] J. F. Ziegler and J. M. Manoyan, Nucl. Instrum. Methods B **35**, 215 (1988).
[22] J. F. Ziegler, Nucl. Instrum. Methods B **219-220**, 1027 (2004).
[23] V. H. Ponce, At. Data Nucl. Data Tables **19**, 63 (1977).
[24] E. Clementi and C. Roetti, At. Data Nucl. Data Tables **14**, 177 (1974).
[25] M. J. Puska and R. M. Nieminen, Phys. Rev. B **27**, 6121 (1983).
[26] N. R. Arista, Nucl. Instrum. Methods B **195**, 91 (2002).
[27] A. Arnau, M. S. Gravielle, J. E. Miraglia, and V. H. Ponce, Phys. Rev. A **67**, 062902 (2003).